REPORT DOCUMENTATION PAGE

AFRL-SR-BL-TR-98-

$0 \, 0668$

1. AGENCY USE ONLY *(Leave blank)*	2. REPORT DATE	3. REPORT TYPE AND DATES COVERED
	31 October 1998	Final Technical Report 15 Nov 97 to 14 Nov 98

4. TITLE AND SUBTITLE
3D In-Situ Stress Analysis of Rock Masses Pertubred by Irregular Topographies and Underground Openings

5. FUNDING NUMBERS
F49620-98-1-0104

6. AUTHOR(S)
Professor Ernian Pan

7. PERFORMING ORGANIZATION NAME(S) AND ADDRESS(ES)
University of Colorado
Department of Mechanical Engineering
Boulder, CO 80309-0427

8. PERFORMING ORGANIZATION REPORT NUMBER

1536606

9. SPONSORING/MONITORING AGENCY NAME(S) AND ADDRESS(ES)
AFOSR/NA
110 Duncan Avenue, Ste B115
Bolling AFB, DC 20332-8050

10. SPONSORING/MONITORING AGENCY REPORT NUMBER

F49620-98-1-0104

11. SUPPLEMENTARY NOTES

12a. DISTRIBUTION AVAILABILITY STATEMENT
Approved for Public Release; Distribution Unlimited.

12b. DISTRIBUTION CODE

13. ABSTRACT *(Maximum 200 words)*
The overall goal of this project is to develop a new and efficient boundary element method (HEM) program for the stress analysis of 3-D anisotropic rock masses that are perturbed by irregular topographies and underground openings. This stress analysis will provide direct information on the best (or optimal) selection of the surface location and hit angle for a penetrator. We have identified three tasks to achieve this goal, which include theoretical and analytical development; computational and numerical development; and laboratory investigation and field validation. This final technical report presents our accomplishments related to the first and second tasks, that is, the theoretical and analytical development, and computational and numerical development.

First, the analytical solution and numerical implementation are presented for elastostatic displacement Green's function for 3D rock masses of general anisotropy. Excerpts from the authors' FORTRAN code are included. A numerical algorithm for the calculation of the derivatives of the Green's displacements and stresses is also introduced. Secondly, these Green's functions are incorporated into a BEM code developed by the authors. Thirdly, numerical results of Green's displacements, stresses and stress derivatives are presented and compared to the closed-form solutions for transversely isotropic rocks. Finally, the BEM code based on the current Green's functions is tested and the numerical results are compared to those using a BEM code based on the exact Green's functions. It is shown that the Green's functions derived in this report are accurate and the corresponding BEM code is correct. This BEM code is now ready for the laboratory comparison and field validation.

14. SUBJECT TERMS
In-situ stres, rock anisotropy, boundary element method, Green's functions.

15. NUMBER OF PAGES
33

16. PRICE CODE

17. SECURITY CLASSIFICATION OF REPORT	18. SECURITY CLASSIFICATION OF THIS PAGE	19. SECURITY CLASSIFICATION OF ABSTRACT	20. LIMITATION OF ABSTRACT
Unclassified	Unclassified	Unclassified	UL

THREE-DIMENSIONAL *IN SITU* STRESS ANALYSIS OF ROCK MASSES PERTURBED BY IRREGULAR TOPOGRAPHIES AND UNDERGROUND OPENINGS

Final Technical Report

for the Grant

AFOSR F49620-98-1-0104

✦ By
Ernian Pan, Research Assistant Professor
Department of Mechanical Engineering
University of Colorado, Boulder, CO 80309-0427
Telephone: (303) 492-7636
Email: pane@spot.colorado.edu

Bernard Amadei, Professor
Department of Civil Engineering
University of Colorado, Boulder, CO 80309-0428
Telephone: (303) 492-7734
Email: amadei@spot.colorado.edu

Abstract

The overall goal of this project is to develop a new and efficient boundary element method (BEM) program for the stress analysis of 3-D anisotropic rock masses that are perturbed by irregular topographies and underground openings. This stress analysis will provide direct information on the best (or optimal) selection of the surface location and hit angle for a penetrator. We have identified three tasks to achieve this goal, which include theoretical and analytical development; computational and numerical development; and laboratory investigation and field validation. This final technical report presents our accomplishments related to the first and second tasks, that is, the theoretical and analytical development, and computational and numerical development.

First, the analytical solution and numerical implementation are presented for elastostatic displacement Green's function for 3D rock masses of general anisotropy. Excerpts from the authors' FORTRAN code are included. A numerical algorithm for the calculation of the derivatives of the Green's displacements and stresses is also introduced. Secondly, these Green's functions are incorporated into a BEM code developed by the authors. Thirdly, numerical results of Green's displacements, stresses and stress derivatives are presented and compared to the closed-form solutions for transversely isotropic rocks. Finally, the BEM code based on the current Green's functions is tested and the numerical results are compared to those using a BEM code based on the exact Green's functions. It is shown that the Green's functions derived in this report are accurate and the corresponding BEM code is correct. This BEM code is now ready for the laboratory comparison and field validation.

1. Introduction

Green's functions are important in the formulation of boundary integral equations and in the solution of those equations by the boundary element method (BEM) [1,2]. In order to handle rock and rock mass anisotropy, the static Green's functions in a 3-D anisotropic full-space are required. Previously, several methods were proposed to calculate these Green's functions. These include the numerical integral method, series expansion technique, dual reciprocity technique, and the eigenvalue/eigenfunction method. While the first three methods are approximate, the last one requires solving a 6x6 eigenvalue system.

After reviewing thoroughly this topic, Wang [3] derived explicit expressions for 3D elastostatic Green's displacements in general anisotropic solids and integrals of Green's displacement derivatives over segments and rectangles.

At the outset, this report reviews some of the basic concepts inherent in Wang's formulation for Green's displacements. A particularized account of the authors' derivation and implementation of these expressions follows, along with the key parts of the authors' own code written in FORTRAN.

Secondly, a numerical algorithm for the calculation of the derivatives of the Green's displacements and stresses is subsequently introduced; it allows the discretization of the boundary to be of the most general type in a BEM formulation.

Thirdly, it is described how the preceding implementations were utilized within a BEM code.

Finally, numerical examples of Green's displacements, stresses and stress derivatives are presented for a transversely isotropic solid, so as to allow a comparison with a previously available closed-form solution [4]. Numerical examples of BEM calculations are also given and the results are compared with exact solutions and previously published numerical results.

2. Outline of the analytical solution

2.1 Notation

Consider the geometry of Figure 1a where (O, x_1, x_2, x_3) is a Cartesian coordinate system in a 3-dimensional Euclidean space R^3, $(\mathbf{u}_1, \mathbf{u}_2, \mathbf{u}_3)$ the corresponding right-handed orthonormal basis and $\mathbf{x}=(x_1, x_2, x_3)$ a point in this space. We assume that the anisotropic body is embedded in this space.

Let $\mathbf{n}=(n_1, n_2, n_3)$ be a vector whose components in R^3 are n_1, n_2, n_3, with respect to $\mathbf{u}_1, \mathbf{u}_2$, $\mathbf{u}_3$, respectively. We can imagine $\mathbf{n}=(n_1, n_2, n_3)$ also as a point in a Cartesian coordinate system of a 3-dimensional Euclidean space, which will be called the $\mathbf{n}$-space. Let Ω be any closed surface containing the origin of the $\mathbf{n}$-space and $d\Omega(\mathbf{n})$ an infinitesimal area element of this surface around point $\mathbf{n}=(n_1, n_2, n_3)$, see Figure 1.b.

Throughout this paper, "$\cdot$" indicates the dot product of two vectors and "$\times$" indicates the cross product. Also, a comma indicates partial differentiation with respect to a variable, i.e. $f_{,i}=\dfrac{\partial f}{\partial x_i}$ and summation over repeated indices is assumed.

2.2 Basic equations

Consider an unbounded homogeneous anisotropic linearly elastic solid subjected to a point load in the fixed coordinate system (O, x_1, x_2, x_3) depicted in Figure 1.a. The Green's function will be denoted by $g_{pk}(\mathbf{x})$ and gives the displacement in the x_p-direction at $\mathbf{x}$ produced by a point load applied at the origin O in the x_k-direction. Let σ_{ij} be the stress tensor, u_i the displacement field and

$$\varepsilon_{pq} = \frac{1}{2}\left(u_{p,q} + u_{q,p}\right) \tag{1a}$$

the infinitesimal strain.

The constitutive relation of linear elasticity reads:

$$\sigma_{ij} = c_{ijpq}\varepsilon_{pq} \tag{1b}$$

where c_{ijpq} is the elastic tensor, which is fully symmetric and positive definite, i.e.:

$$c_{ijpq} = c_{jipq} = c_{ijqp} = c_{pqij} \tag{1c}$$

$$c_{ijpq}a_{ij}a_{pq} > 0 \qquad \forall \text{ non-zero tensor } a_{ij} \tag{1d}$$

Inserting the kinematics relation (1a) into the constitutive relation (1b) and the latter into the equilibrium equation:

$$\sigma_{ij,j} + F_i = 0 \tag{2a}$$

where F_i is the body force per unit volume, we obtain the following three second-order partial differential equations:

$$c_{ijpq}u_{p,jq} + F_i = 0 \tag{2b}$$

once the symmetry (1c) of the elastic tensor is taken into account. Because the Green's function is relative to a point force, (2b) becomes:

$$c_{ijpq}g_{pk,jq}(\mathbf{x}) = -\delta_{ik}\delta(\mathbf{x}) \tag{3}$$

where δ_{ik} is the Kronecker delta and $\delta(\mathbf{x})$ the Dirac delta.

In the subsequent implementation, the 6x6 matrix $\mathbf{D}$ of Voigt constants is introduced such that:

$$\sigma_k = \mathbf{D}\,\varepsilon_k \tag{4}$$

where $\sigma_k = (\sigma_{11k}, \sigma_{22k}, \sigma_{33k}, \sigma_{23k}, \sigma_{13k}, \sigma_{12k})^T$ is the Green's stress vector (relative to a point force applied in direction k at the origin) and $\varepsilon_k = (\varepsilon_{11k}, \varepsilon_{22k}, \varepsilon_{33k}, 2\varepsilon_{23k}, 2\varepsilon_{13k}, 2\varepsilon_{12k})^T$ is the Green's strain vector (relative to a point force applied in direction k at the origin) with its components being defined as :

$$\varepsilon_{ijk} = \frac{1}{2}\left(g_{ik,j} + g_{jk,i}\right) \tag{5}$$

The following rules apply between the components c_{ijks} and $D_{\alpha\beta}$ and account for the first two symmetries of formula (1c) [5]:

If $i=j$, $\alpha=i$; $\tag{6}$

If $i\neq j$, $\alpha=9-i-j$; $\tag{7}$

If $k=s$, $\beta=k$; $\tag{8}$

If $k\neq s$, $\beta=9-k-s$; $\tag{9}$

The third symmetry of formula (1c) is accomplished by the symmetry of $\mathbf{D}$, therefore:

If $\alpha\leq\beta$, $c_{ijks} = D_{\alpha\beta}$; $\tag{10}$

If $\alpha>\beta$, $c_{ijks} = D_{\beta\alpha}$; $\tag{11}$

2.3 Analytic solution

We notice that $c_{ijpq}n_jn_q$ is symmetric and positive definite, so that it's inverse is well defined. We set:

$$\Gamma_{ip}(\mathbf{n}) = c_{ijpq}n_jn_q \; ; \quad \Gamma_{ip}^{-1}(\mathbf{n}) = \left(c_{ijpq}n_jn_q\right)^{-1} \tag{12}$$

Consider now the following identities, in which integration is taken in the $\mathbf{n}$-space over any closed surface Ω including the origin (see Figure 1b) and use is made of Eqs. (A.6b) and (A.8) (see Appendix A):

$$c_{irps} \frac{\partial^2}{\partial x_r \partial x_s} \int_\Omega \Gamma_{pk}^{-1}(\mathbf{n}) \delta(\mathbf{n} \cdot \mathbf{x}) d\Omega(\mathbf{n}) = c_{irps} \int_\Omega \Gamma_{pk}^{-1}(\mathbf{n}) n_r n_s \left. \frac{d^2 \delta(s)}{ds^2} \right|_{s=\mathbf{n} \cdot \mathbf{x}} d\Omega(\mathbf{n}) =$$

$$= \int_\Omega c_{irps} n_r n_s \left(c_{prqs} n_r n_s \right)^{-1} \left. \frac{d^2 \delta(s)}{ds^2} \right|_{s=\mathbf{n} \cdot \mathbf{x}} d\Omega(\mathbf{n}) = \delta_{ik} \int_\Omega \left. \frac{d^2 \delta(s)}{ds^2} \right|_{s=\mathbf{n} \cdot \mathbf{x}} d\Omega(\mathbf{n}) = \qquad (13)$$

$$= \delta_{ik} \nabla \int_\Omega \frac{\delta(\mathbf{n} \cdot \mathbf{x})}{|\mathbf{n}|^2} d\Omega(\mathbf{n})$$

Since the last member in (13) can be written in terms of the plane representation of the delta function (A.10), we have:

$$c_{irps} \frac{\partial^2}{\partial x_r \partial x_s} \int_\Omega \Gamma_{pk}^{-1}(\mathbf{n}) \delta(\mathbf{n} \cdot \mathbf{x}) d\Omega(\mathbf{n}) = -8\pi^2 \delta_{ik} \delta(\mathbf{x}) \qquad (14)$$

By comparing (3) with (14), we get the following integral expression for the Green's displacement function:

$$g_{pk}(\mathbf{x}) = \frac{1}{8\pi^2} \int_\Omega \Gamma_{pk}^{-1}(\mathbf{n}) \delta(\mathbf{n} \cdot \mathbf{x}) d\Omega(\mathbf{n}) \qquad (15)$$

We now try to write (15) in a form suitable for integration by means of the Theory of Residues [6]. To this end, we express the inverse tensor $\Gamma_{pk}^{-1}(\mathbf{n})$ as:

$$\Gamma_{pk}^{-1}(\mathbf{n}) = \frac{A_{pk}(\mathbf{n})}{D(\mathbf{n})} \qquad (16)$$

where $A_{pk}(\mathbf{n})$ is the adjoint matrix of $c_{ijpq} n_j n_q$ and $D(\mathbf{n})$ is the determinant of $c_{ijpq} n_j n_q$, e.g.:

$$A_{pk}(\mathbf{n}) = adj \lfloor c_{ijpq} n_j n_q \rfloor ; \qquad D(\mathbf{n}) = \det \lfloor c_{ijpq} n_j n_q \rfloor \qquad (17)$$

It is convenient to use coordinates (ξ, ζ, η) introduced in Appendix B. Using Eq. (B.4), equation (15) becomes:

$$g_{pk}(\mathbf{x}) = \frac{1}{8\pi^2} \int_\Omega \frac{A_{pk}(\xi \mathbf{p} + \zeta \mathbf{q} + \eta \mathbf{e})}{D(\xi \mathbf{p} + \zeta \mathbf{q} + \eta \mathbf{e})} \delta(r\eta) d\Omega(\xi, \zeta, \eta) \qquad (18)$$

where r is the distance between the field and source points (see equation (B.1.a)).

Since $\Gamma_{pk}(\mathbf{n})$ is a 3x3 matrix, each entry of its adjoint matrix A_{pk} is a polynomial of order 4 in ξ, ζ and η. Similarly, determinant $D(\mathbf{n})$ is a polynomial of order 6 in ξ, ζ and η.

Following Wang [3], we choose Ω as a rectangular parallelepiped having size 2Lx2Lx2 (Fig. 2) and let the dimension L go to infinity. Since over surfaces other than S_1 and S_2 the integrand in (18) approaches zero as $1/L^2$, the contribution of the integration over every surface but S_1 and S_2 vanishes. Moreover, the integrand in (18) is symmetric with respect to ξ, since only even powers of ξ are involved. This leads to twice the integration over S_1 ($\xi=1$):

$$g_{pk}(\mathbf{x}) = \frac{1}{4\pi^2} \int_{S_1} \frac{A_{pk}(\mathbf{p} + \zeta\mathbf{q} + \eta\mathbf{e})}{D(\mathbf{p} + \zeta\mathbf{q} + \eta\mathbf{e})} \delta(r\eta) d\Omega(\xi,\zeta,\eta) =$$

$$= \frac{1}{4\pi^2} \int_{-\infty}^{\infty} \int_{-\infty}^{\infty} \frac{A_{pk}(\mathbf{p} + \zeta\mathbf{q} + \eta\mathbf{e})}{D(\mathbf{p} + \zeta\mathbf{q} + \eta\mathbf{e})} \delta(r\eta) d\zeta d\eta \qquad (19)$$

We recall that [6], for any infinitely differentiable function $f(x)$ and any positive real number α:

$$\int_{-\infty}^{\infty} \delta(\alpha x) f(x) dx = \frac{1}{\alpha} \int_{-\infty}^{\infty} \delta(x) f(x/\alpha) dx = \frac{1}{\alpha} f(0) \qquad (20)$$

which is justified by the change of variables $\alpha x \rightarrow x$. Therefore, integrating (19) with respect to η yields :

$$g_{pk}(\mathbf{x}) = \frac{1}{4\pi^2 r} \int_{-\infty}^{\infty} \frac{A_{pk}(\mathbf{p} + \zeta\mathbf{q})}{D(\mathbf{p} + \zeta\mathbf{q})} d\zeta \qquad (21)$$

The integral in (21) can be handled by means of the Theory of the Residues [6]. The poles are the roots of the polynomial equation of sixth order in ζ:

$$D(\mathbf{p} + \zeta\mathbf{q}) = 0 \qquad (22)$$

If $\mathbf{n} \neq 0$ is real, $\Gamma_{pk}(\mathbf{n})$ is a real symmetric, positive definite matrix and then its eigenvalues are all real and positive [6], thus its determinant can never be zero. If we want Eq. (22) to be satisfied, ζ must therefore be complex. A corollary of the Fundamental Theorem of Algebra [7] tells us that a real polynomial of order N has N roots and that if $\zeta = a + ib$ is a root, its conjugate $\zeta^* = a - ib$ must also be a root [7]. In our case we have 3 roots ζ_m satisfying :

$$D(\mathbf{p} + \zeta_m\mathbf{q}) = 0 \qquad (23)$$

with:

$$\mathrm{Im}\,\zeta_m > 0 \qquad m=1,2,3 \qquad (24)$$

and we may write:

$$D(\mathbf{p} + \zeta\mathbf{q}) = \sum_{k=0}^{6} a_{k+1}\zeta^k = a_7 \prod_{m=1}^{3} (\zeta - \zeta_m)(\zeta - \zeta_m^*) \qquad (25)$$

where a_k are the coefficients of the sextic polynomial $D(\mathbf{p} + \zeta\mathbf{q})$ with respect to ζ. Equation (23) is called the sextic equation of elasticity and it has been shown that no closed-form solution exists for its roots [8]. Thus this equation must be solved numerically. Integral (21) can now be expressed in terms of the residues at the poles, taking into account that it must be real:

$$g_{pk}(\mathbf{x}) = -\frac{\mathrm{Im}}{2\pi r} \sum_{m=1}^{3} \frac{A_{pk}(\mathbf{p} + \zeta_m\mathbf{q})}{a_7(\zeta_m - \zeta_m^*) \prod_{\substack{k=1 \\ k \neq m}}^{3} (\zeta_m - \zeta_k)(\zeta_m - \zeta_k^*)} \qquad (27)$$

6

It is the authors' experience that the 6 poles resulted simple even with isotropic materials. Should the poles be multiple, a slight change in the elastic constants will result in single poles, with negligible errors in the computed Green's tensor.

Some features of formula (27) need to be pointed out:

1) since $\Gamma_{pk}(\mathbf{n})$ is symmetric, its adjoint matrix A_{pk} is also symmetric and so is Green's tensor g_{pk}. As a consequence, only 6 terms out of 9 must be calculated;

2) for two points $\mathbf{x}_1$ and $\mathbf{x}_2$ aligned along the same line passing through the origin, the summation over index m has the same value;

3) as a consequence of 2), g_{pk} approaches zero as $1/r$ when $r \to \infty$;

4) as a consequence of 2), g_{pk} depends only on the relative position of the source point and field point. Thus the implementation can proceed considering the source point always at the origin, by an applicable translation; this leads to an important simplification of the implementation itself;

5) the numerical solution of a polynomial of sixth order is the only numerical step required in order to obtain the entire Green's function.

3. Implementation of the analytic solution

The key steps in the implementation of the analytic formulation fall essentially into two groups:

1) entries of $\Gamma_{ij}(\mathbf{p} + \zeta\mathbf{q})$ in terms of stiffness matrix components $D_{\alpha\beta}$, coordinates of field point $\mathbf{x}$, and variable ζ;

2) coefficients a_i $i=1,...,7$ of sextic polynomial (25).

In order to keep the expressions as simple as possible, vector $\mathbf{v}$ introduced in Appendix B must coincide with one of the base vectors $\mathbf{u}_1$, $\mathbf{u}_2$, $\mathbf{u}_3$. In the following, we have assumed that $\mathbf{v}$ is either $(1,0,0)$ or $(0,1,0)$; the choice between them must be done on the basis of $\mathbf{x}$ and affects step 1) only.

3.1 Entries of matrix $\Gamma_{ij}(\mathbf{p} + \zeta\mathbf{q})$

Each entry of matrix $\Gamma_{ij}(\mathbf{p} + \zeta\mathbf{q})$ is a polynomial of order two in ζ of the form:

$$\Gamma_{ij}(\mathbf{p} + \zeta\mathbf{q}) = b_{ij1} + b_{ij2}\zeta + b_{ij3}\zeta^2 \qquad (28)$$

As an example, coefficients b_{ijk} are given in Appendix C in FORTRAN format for the case $\mathbf{v}=(1,0,0)$; they take into account Eqs. (6)-(11) so that they are functions of the entries of matrix $\mathbf{D}$, which are much more manageable then the fourth-order tensor c_{ijpq}. Coefficients b_{ijk} are also functions of the field point coordinates. The correspondence between notation used in the text and notation used in the Fortran code is established in Table 1. Mathematica 2.2 was used to get the expression of coefficients b_{ijk}.

3.2 Coefficients of the sextic polynomial

Although it is possible to get the expressions of coefficients a_i ($i=1,...,7$) directly in terms of the stiffness matrix components $D_{\alpha\beta}$ and of the field point coordinates, this leads to expressions as long as 40 pages, which cannot be handled easily by the compiler and are not computationally efficient. Thus the idea is to derive them in terms of the b_{ijk} coefficients introduced in (28). Determinant $D(\mathbf{p} + \zeta\mathbf{q})$ can in fact be written as the sum of trinomials:

$$D(\mathbf{p}+\zeta\mathbf{q})=-\Gamma_{13}\Gamma_{22}\Gamma_{31}+2\Gamma_{12}\Gamma_{23}\Gamma_{31}-\Gamma_{11}\Gamma_{23}\Gamma_{32}-\Gamma_{12}\Gamma_{21}\Gamma_{33}+\Gamma_{11}\Gamma_{22}\Gamma_{33} \qquad (29)$$

If we put (28) into (29), we realize that each coefficient a_i (relative to ζ^{i-1}) is a sum of trinomials of b_{ijk} coefficients. Let l, m, n be the last indexes of the coefficients of a trinomial, we found that these indexes have to satisfy $l + m + n = i-2$ in order for the product to be of order $i-1$. For example, only coefficients b_{ijk} such that $k=1$ contribute to a_1. Thus, in general :

$$a_i = -\sum_{l,m,n:l+m+n=i-2}b_{13i}b_{22j}b_{31k} + 2\sum_{l,m,n:l+m+n=i-2}b_{12i}b_{23j}b_{31k} - \sum_{l,m,n:l+m+n=i-2}b_{11i}b_{23j}b_{32k} -$$
$$- \sum_{l,m,n:l+m+n=i-2}b_{12i}b_{21j}b_{33k} + \sum_{l,m,n:l+m+n=i-2}b_{11i}b_{22j}b_{33k} \qquad (30)$$

Coefficients a_i calculated according to (30) are given in Appendix D in Fortran format (see Table 1 for notation correspondence). It is to be noted that the present implementation of the analytic solution is quite simple, when compared to the complexity of the problem in hand.

4. Derivatives of the Green's displacements and stresses

Analytic solutions for the integral over segments and rectangles of the Green's displacement derivatives were proposed by Wang [3]. However, expressions of the derivatives of the Green's displacements are necessary if the boundary discretization must be more general. Several attempts were made by the authors in order to get a closed form solution of the Green's function derivatives. The most promising of them started from the derivation of (21) and led to the expression :

$$g_{pk,s}(\mathbf{x}) = \frac{x_s}{2\pi r^3}\mathrm{Im}\sum_{m=1}^{3}\frac{A_{pk}(\mathbf{p}+\zeta_m\mathbf{q})}{a_7(\zeta_m-\zeta_m{}^*)\prod_{\substack{k=1\\k\neq m}}^{3}(\zeta_m-\zeta_k)(\zeta_m-\zeta_k{}^*)} -$$

$$-\frac{1}{2\pi r}\mathrm{Im}\sum_{m=1}^{3}\frac{\dfrac{\partial A_{pk}(\mathbf{p}+\zeta_m\mathbf{q})}{\partial x_s}}{a_7(\zeta_m-\zeta_m{}^*)\prod_{\substack{k=1\\k\neq m}}^{3}(\zeta_m-\zeta_k)(\zeta_m-\zeta_k{}^*)} + \qquad (31)$$

$$+\frac{1}{2\pi r}\mathrm{Im}\sum_{m=1}^{3}\lim_{\zeta\to\zeta_m}\frac{d}{d\zeta}\left[(\zeta-\zeta_m)^2\frac{A_{pk}}{D^2}\frac{\partial D}{\partial x_s}\right]$$

In this equation, the last term is very complicated, therefore, a numerical algorithm was implemented based on the Lagrange polynomials [9]. Despite of its simplicity, this approach has been proven to be efficient, accurate, and robust.

Following [9], let a function $f(x)$ be known at the n points $x_1 < x_2 < ... < x_n$. Let us call $y_i = f(x_i)$ $i=1,...,n$ and set :

$$F(x) = \prod_{k=1}^{n}(x-x_k) ; \quad F_k(x) = \prod_{\substack{r=1\\r\neq k}}^{n}(x-x_r) ; \quad F_k(x_k) = \prod_{\substack{r=1\\r\neq k}}^{n}(x_k-x_r) \qquad (32)$$

The complete Lagrange interpolation function is :

$$f(x) = P(x) + F(x) \cdot \frac{f^{(n)}(\xi(x))}{n!}$$ (33)

where :

$$P(x) = \sum_{k=1}^{n} \frac{F_k(x)}{F_k(x_k)} \cdot y_k$$ (34)

By taking the derivative of (33) and evaluating it in x_r, we get :

$$f'(x_r) = P'(x_r) + F'(x_r) \cdot \frac{f^{(n)}(\xi(x_r))}{n!}$$ (35)

Thus, the error in the first derivative is :

$$F'(x_r) \cdot \frac{f^{(n)}(\xi(x_r))}{n!}$$ (36)

$F'(x_r)$ is nothing but the product of the distances between x_r and the other chosen abscissas. Therefore, if the intervals between the chosen abscissas is constant, its minimum value is attained at the mid point (or two mid-points if n is even) of the segment between x_1 and x_n. It follows that the best approximation of the value of $f'(x_r)$ obtainable using the polynomial derivative is attained at the mid point (or two mid points if n is even) of the segment between x_1 and x_n.
It can be shown that the derivative of the Lagrange polynomial is [9]:

$$P'(x_r) = \sum_{\substack{k=1 \\ k \neq r}}^{n} \frac{1}{x_r - x_k} \left[y_r - y_k \frac{F'(x_r)}{F'(x_k)} \right]$$ (37)

If we choose a polynomial of order 2, i.e. 3 abscissas, from (35) and (37) we get:

$$f'(x_2) = \frac{1}{2h} [-f(x_1) + f(x_3)] - \frac{h^2}{6} f^{(3)}(\xi_2)$$ (38)

where h is the distance between two consecutive abscissas and ξ_2 is a point comprised between x_1 and x_3.

Now, let $\mathbf{x}$ be the field point at which we want to calculate the Green's stress component σ_{ijk} defined in Section 2.2. To this end, the expression of the Green's strain component ε_{ijk} at $\mathbf{x}$ is necessary in order to calculate σ_{ijk} by means of (4). Using (38), the following expressions of the Green's strain component ε_{ijk} at $\mathbf{x}$ are obtained:

$$\varepsilon_{11k}(\mathbf{x}) \approx \frac{g_{1k}(\mathbf{x}+\Delta_1) - g_{1k}(\mathbf{x}-\Delta_1)}{2h}$$ (39)

$$\varepsilon_{22k}(\mathbf{x}) \approx \frac{g_{2k}(\mathbf{x}+\Delta_2) - g_{2k}(\mathbf{x}-\Delta_2)}{2h}$$ (40)

$$\varepsilon_{33k}(\mathbf{x}) \approx \frac{g_{3k}(\mathbf{x}+\Delta_3) - g_{3k}(\mathbf{x}-\Delta_3)}{2h}$$ (41)

$$\varepsilon_{23k}(\mathbf{x}) \approx \frac{g_{3k}(\mathbf{x}+\Delta_2)-g_{3k}(\mathbf{x}-\Delta_2)+g_{2k}(\mathbf{x}+\Delta_3)-g_{2k}(\mathbf{x}-\Delta_3)}{2h} \tag{42}$$

$$\varepsilon_{13k}(\mathbf{x}) \approx \frac{g_{1k}(\mathbf{x}+\Delta_3)-g_{1k}(\mathbf{x}-\Delta_3)+g_{3k}(\mathbf{x}+\Delta_1)-g_{3k}(\mathbf{x}-\Delta_1)}{2h} \tag{43}$$

$$\varepsilon_{12k}(\mathbf{x}) \approx \frac{g_{1k}(\mathbf{x}+\Delta_2)-g_{1k}(\mathbf{x}-\Delta_2)+g_{2k}(\mathbf{x}+\Delta_1)-g_{2k}(\mathbf{x}-\Delta_1)}{2h} \tag{44}$$

where $\Delta_1=(h,0,0)$, $\Delta_2=(0, h, 0)$, $\Delta_3=(0,0, h)$.

In order to get the complete Green's stress and strain at point $\mathbf{x}$, it is thus necessary to compute the Green's tensor at 6 points in the neighborhood of $\mathbf{x}$. The choice of interval h is a crucial decision. An extensive numerical investigation has led us to the conclusion that the best value of the interval is:

$$h = r \cdot 10^{-6} \tag{45}$$

where r is the distance between the field and source points.

It is also noteworthy that the attempts aimed at increasing the accuracy of the approximation by adding other terms to (39)-(44) led to no appreciable improvement. In the authors' opinion, the reason for the good performance of this scheme lies primarily in the smooth and monotonic behavior of the Green's displacements.

In order to calculate internal stresses, the derivatives of the Green's stresses and displacements are needed with respect to the coordinates of the source point (see Section 5). By virtue of Observation 4 in Section 2, these derivatives are equal but opposite in sign to the derivatives taken with respect to the field point x_i. According to (38), the derivatives of the Green's stresses are approximated as:

$$\sigma_{ijk,l}(\mathbf{x}) \approx \frac{\sigma_{ijk}(\mathbf{x}+\Delta_l)-\sigma_{ijk}(\mathbf{x}-\Delta_l)}{2h} \qquad l=1,2,3 \tag{46a}$$

and the derivatives of the Green's displacements as:

$$g_{ij,l}(\mathbf{x}) \approx \frac{g_{ij}(\mathbf{x}+\Delta_l)-g_{ij}(\mathbf{x}-\Delta_l)}{2h} \qquad l=1,2,3 \tag{46b}$$

5. BEM formulation

Consider an elastic body (finite or infinite) with the following displacement and traction conditions imposed on the boundary $\Gamma=\Gamma_u+\Gamma$:

$$u_j(\mathbf{x})=\bar{u}_j(\mathbf{x}) \qquad \mathbf{x} \in \Gamma_u \tag{47a}$$

$$\sigma_{ij}(\mathbf{x})n_j(\mathbf{x})=\bar{T}_j(\mathbf{x}) \qquad \mathbf{x} \in \Gamma_t \tag{47b}$$

with n_j being the external normal to Γ_t.

For each internal point $\mathbf{x}_p$ the following integral equation holds [10]:

$$u_i(\mathbf{x}_p) + \int_\Gamma T_{ij}^*(\mathbf{x}_p,\mathbf{x}) u_j(\mathbf{x}) d\Gamma(\mathbf{x}) = \int_\Gamma U_{ij}^*(\mathbf{x}_p,\mathbf{x}) T_j(\mathbf{x}) d\Gamma(\mathbf{x}) \tag{48}$$

where $U_{ij}^*(\mathbf{x}_p,\mathbf{x})$ and $T_{ij}^*(\mathbf{x}_p,\mathbf{x})$ are the Green's displacements and tractions, respectively. By virtue of Observation 4 in Section 2, $U_{ij}^*(\mathbf{x}_p,\mathbf{x})$ and $T_{ij}^*(\mathbf{x}_p,\mathbf{x})$ are equal to:

$$U_{ij}^*(\mathbf{x}_p,\mathbf{x}) = g_{ij}(\mathbf{x}-\mathbf{x}_p) \tag{49}$$

$$T_{ij}^*(\mathbf{x}_p,\mathbf{x}) = \sigma_{jkj}(\mathbf{x}-\mathbf{x}_p) n_k(\mathbf{x}) \tag{50}$$

If $\mathbf{x}_p$ approaches a point $\mathbf{x}_b$ on the boundary, (48) is modified as:

$$d_{ij} u_j(\mathbf{x}_b) + \int_\Gamma T_{ij}^*(\mathbf{x}_b,\mathbf{x}) u_j(\mathbf{x}) d\Gamma(\mathbf{x}) = \int_\Gamma U_{ij}^*(\mathbf{x}_b,\mathbf{x}) T_j(\mathbf{x}) d\Gamma(\mathbf{x}) \tag{51}$$

where d_{ij} are coefficients that depend only on the local geometry of the boundary at $\mathbf{x}_b$.

The term on the right-hand side of (51) has weak singularity (see Observation 3, Section 2) and can thus be integrated by means of a usual Gauss quadrature technique. The rigid-body motion method [11] can be used to overcome the Cauchy-type singularity in the first integrand and at the same time to avoid the calculation of coefficients d_{ij}.

Equation (51) can be discretized and, once boundary conditions (47) are taken into account, the resulting algebraic system of equations can be solved for the unknown boundary displacements and tractions. Then Eq. (48) can be used to calculate internal displacements.

In order to get the internal stresses, it is necessary to take the derivative of (48) with respect to the internal coordinates $\mathbf{x}_p$. This yields:

$$u_{i,l}(\mathbf{x}_p) + \int_\Gamma T_{ij,l}^*(\mathbf{x}_p,\mathbf{x}) u_j(\mathbf{x}) d\Gamma(\mathbf{x}) = \int_\Gamma U_{ij,l}^*(\mathbf{x}_p,\mathbf{x}) T_j(\mathbf{x}) d\Gamma(\mathbf{x}) \tag{52}$$

where:

$$T_{ij,l}^*(\mathbf{x}_p,\mathbf{x}) = -\sigma_{ikj,l}(\mathbf{x}-\mathbf{x}_p) n_k(\mathbf{x}) \tag{53a}$$

$$U_{ij,l}^*(\mathbf{x}_p,\mathbf{x}) = -g_{ij,l}(\mathbf{x}-\mathbf{x}_p) \tag{53b}$$

with $\sigma_{ikj,l}(\mathbf{x}-\mathbf{x}_p)$ given by (46a) and $g_{ij,l}(\mathbf{x}-\mathbf{x}_p)$ by (46b).

Once $u_{i,l}(\mathbf{x}_p)$ are obtained, the internal stresses are calculated by means of the following equation similar to (4) and (5):

$$\sigma = \mathbf{D}\,\varepsilon \tag{54a}$$

where:

$$\sigma = (\sigma_{11}, \sigma_{22}, \sigma_{33}, \sigma_{23}, \sigma_{13}, \sigma_{12})^T \tag{54b}$$

$$\varepsilon = (\varepsilon_{11}, \varepsilon_{22}, \varepsilon_{33}, 2\varepsilon_{23}, 2\varepsilon_{13}, 2\varepsilon_{12})^T \tag{54c}$$

$$\varepsilon_{ij} = \frac{1}{2}(u_{i,j} + u_{j,i}) \tag{54d}$$

11

The implementation described in Sections 3 and 4 was incorporated into an existing 3D BEM code (see [11] for its description) according to the procedure presented in this Section.

6. Numerical examples

6.1 Green's displacements, stresses and derivatives of the stresses

Let us consider a transversely isotropic and linearly elastic solid, whose plane of transverse isotropy is parallel to the x_1x_2 plane. A closed-form solution exists in this case [4] for the Green's displacements, stresses and derivatives of the stresses. This solution will be used (as implemented in [11]) to validate the proposed formulation.

The material properties are as follows: $E=20 \cdot 10^4$ kN/m^2, $E'=4 \cdot 10^4$ kN/m^2, $v=0.25$, $v'=0.25$, $G'=1.6 \cdot 10^4$ kN/m^2, where E and E' are the Young's modulus in the plane of transverse isotropy and in the direction normal to it, respectively; v and v' are the Poisson's ratios characterizing the lateral strain response in the plane of transverse isotropy to a stress acting parallel and normal to it, respectively; G' is the shear modulus in planes normal to the plane of symmetry. The corresponding stiffness matrix D is (only the upper half is given):

$$\begin{pmatrix} 88 & 72 & 40 & 0 & 0 & 0 \\ & 88 & 40 & 0 & 0 & 0 \\ & & 24 & 0 & 0 & 0 \\ & & & 16 & 0 & 0 \\ & sym. & & & 16 & 0 \\ & & & & & 8 \end{pmatrix} \cdot 10^4 \text{ kN/m}^2 \tag{55}$$

The field point is placed at $x=(-1,0.8,1.5)$ m. The displacements, stresses, stress derivatives are collected in Tables 2, 3 and 4, respectively. The agreement between the closed-form solution and the present formulation is very good for all three quantities. Only for some components of the derivatives of the stresses (Table 4) is the relative difference not negligible; however, it must be noted that the magnitude of these components is small with respect to the remaining components, thus leading to negligible errors in the computation of the internal stresses, as will be shown in Section 6.2.

6.2 BEM models

The geometry of the following two examples is the same. A cube of transversely isotropic material, whose edge is 1m long, is discretized very coarsely with 6 nine-node isoparametric elements and with a total of 26 nodes (see Figure 3). The faces of the block are parallel to the coordinate planes. The block is subjected to uniform compression of 1 kN/m^2 on the two faces parallel to the x_1x_2 plane. For this case, an exact solution exists [12].

In the first example we adopt the same material constants as considered in Section 6.1. However, the plane of symmetry is no longer parallel to the x_1x_2 plane, but is inclined with dip orientation $\varphi=60°$ and dip angle $\psi=45°$ (see Figure 4). Consequently, stiffness matrix D referred to x_1, x_2, x_3 axes is now fully populated (only the upper half is given):

12

$$
\begin{pmatrix}
14.5 & 9.9 & 9.6 & -0.2 & -3.1177 & -1.5588 \\
 & 18.5 & 9.6 & -2.2 & -1.0392 & -1.9052 \\
 & & 12.8 & -1.6 & -2.7713 & 0 \\
 & & & 3.2 & 0 & -1.0392 \\
 & sym. & & & 3.2 & -0.2 \\
 & & & & & 3.5
\end{pmatrix} \cdot 10^4 \, \text{kN/m}^2
\qquad (56)
$$

This case was also considered in [11] where it was solved using the closed-form solution for the Green's displacements, stresses and stress derivatives by Pan and Chou [4]. The results obtained with these formulations and with the present one are given in Tables 5 and 6; they indicate that for both the displacements (on the boundary and internal) and internal stresses, the exact values and the values calculated in [11] are in very good agreement.

The second example resembles the one reported in [13]. Here a (transversely isotropic) zinc cube is considered, whose plane of symmetry is parallel to the $x_1 x_2$ plane. The stiffness matrix referred to x_1, x_2, x_3 axes is now (only the upper half is given):

$$
\begin{pmatrix}
161.00 & 34.20 & 50.10 & 0 & 0 & 0 \\
 & 161.00 & 50.10 & 0 & 0 & 0 \\
 & & 61.00 & 0 & 0 & 0 \\
 & & & 38.3 & 0 & 0 \\
 & & & & 38.30 & 0 \\
 & & & & & 63.40
\end{pmatrix} \text{GPa}
\qquad (57)
$$

It is to be noted that zinc has a negative Poisson ratio ν_{12}=-0.06. In Table 7 the results obtained by Schclar [13] with a different numerical formulation for general anisotropic bodies are given in the second column. Form a comparison between columns 1 and 3 and 2 and 3, it turns out that the present formulation and implementation is much more precise.

7. Conclusions

The implementation of an analytic solution for Green's displacements in general anisotropic solids is presented. Its detailed illustration has been accompanied with excerpts from the authors' own Fortran code, in order for the implementation to be available and readily usable by as many readers as possible. Many features distinguish the present implementation from the existing numerical formulations:

1) the procedure is completely analytic, the only numerical step is represented by the determination of the roots of a sixth-order polynomial;
2) once the roots of this polynomial are known, the entire Green's tensor is immediately calculated;
3) the procedure is very robust, since no problem arose even with highly degenerate materials such as transversely isotropic or isotropic materials;
4) the implementation is very efficient, since less than 16 sec were necessary to run 10,000 calculations of the entire Green's tensor in a PC featuring a 266 Mhz Pentium II processor and 64 MB RAM;
5) an extensive numerical validation (one example of which was included in the paper) has shown its high accuracy.

A numerical algorithm has also been proposed for the Green's stresses and their derivatives. Despite its simplicity, it has been proven to be:

1) robust, since no problem arose even with highly degenerate materials such as transversely isotropic or isotropic materials;
2) very accurate even with degenerate materials and/or when the field point is very close to or very far from the source point ;
3) very efficient, since less than 80 sec were necessary to run 10.000 calculations of the complete Green's stresses in a PC featuring a 266 MHz Pentium II processor and 64 MB RAM.

Finally, the performance of the proposed implementations within a previously developed 3D BEM code [11] turned out to be highly accurate when compared to both exact solutions and transversely isotropic BEM formulations for which the closed-form expressions of the Green's displacements, stresses and stress derivatives were used. When compared to previously published results obtained with completely numerical formulations, the present implementation turned out to be much more precise.

In conclusion, the anisotropic Green's functions and the corresponding 3D BEM code are accurate and efficient. The authors are currently investigating the effect of rock anisotropy, irregular topography, and underground openings on the 3D in-situ stresses. The outcome of such an analysis could have application in some of the air force projects, in particular, in the penetration mechanics related project.

8. Acknowledgment/Disclaimer

9. References

1. Synge, J. L. *The Hypercircle in Mathematical Physics*. Cambridge University Press, Cambridge, UK, 1957.

2. Mura, T. *Micromechanics and Defects in Solids - 2nd edition*. Martinus Nijhoff, 1987.

3. Wang, C.-Y. Elastic fields produced by a point source in solids of general anisotropy. *J. Eng. Math.* 1997, **32**, 41-52.

4. Pan, Y. C. and Chou, T. W. Point force solution for an infinite transversely isotropic solid. *J. Appl. Mech.* 1976, **29**, 225-236.

5. Ting, T. C. T. *Anisotropic Elasticity - Theory and Applications*. Oxford University Press, New York, 1996.

6. Wylie, C. R. and Barrett, L. C. *Advanced Engineering Mathematics - 6th Edition*. McGraw Hill, New York, 1995.

7. Barozzi, E. and Gonzales, E. *Calculus* - Vol. 1.Edizioni Libreria Progetto, Padova, 1989.

8. Head, A. K.. The Gaois unsolvability of the sextic equation of anisotropic elasticity. *J. Elasticity* 1979, **9**, pp. 9-20.

9. Gambolati, G. *Elementi di Calcolo Numerico - 3rd edition*. Edizioni Libreria Cortina, Padova, Italy, 1988.

10. Brebbia, C. A. and Domininguez, J. *Boundary Elements, An Introductory Course*. McGraw Hill, New York, 1989.

11. Pan, E. and Amadei, B. 3-D boundary element formulation of anisotropic elasticity with gravity. *Appl. Math. Modeling* 1996, **20**: 114-120.

12. Lekhnitskii, S. G. *Theory of Elasticity of an Anisotropic Elastic Body*. Holden-Day, San Francisco, 1963.

13. Schclar, N. A. *Anisotropic Analysis Using Boundary Elements*. Topics in Engineering Volume 20. Computational Mechanics Publications, Southampton, UK, 1994.

14. Deans, S. R. *The Radon Transform and Some of Its Applications*. Wiley-Interscience Publication, New York,1983.

15. John, F.. *Plane Waves and Spherical Means Applied to Partial Differential Equations*. Interscience, New York, 1955.

16. Ludwig, D. The Radon Transform on Euclidean space. *Comm. Pure Appl. Math.* 1966, **19**, pp. 49-81.

17. Gel'fand, I. M., Graev, M. I. and Vilenkin, Y. N. *Generalized Functions, Vol.5*. Academic Press, New York, 1966.

18. Helgason, S. *The Radon Transform*. Birkhauser, Boston, Basel, Stuttgard, 1980.

19. Courant, R. and Hilbert, D. *Methods of Mathematical Physics, Vol. II*. Interscience Publishers Inc., New York, 1962.

10. Appendix A: Radon Transform and plane representation of the Dirac delta function

The Radon Transform ([14]-[19]) is of fundamental importance in order to work out the analytic solution of the problem at hand.

Let $f(\mathbf{x})$ be a function defined in R^3 and s a real number; the Radon transform of $f(\mathbf{x})$ is defined as :

$$\hat{f}(s,\mathbf{n}) = R[f(\mathbf{x})] = \int f(\mathbf{x}) \cdot \delta(s - \mathbf{n} \cdot \mathbf{x}) d\mathbf{x} \qquad (A.1)$$

where $\delta()$ is the one-dimensional Dirac delta function.

It follows that, when s varies over the real line, the Radon transform is an integration of $f(\mathbf{x})$ over all planes defined by $\mathbf{n} \cdot \mathbf{x} = s$, i.e. having normal $\mathbf{n}$ and distant $s/|\mathbf{n}|$ from the origin O.

The *inverse Radon transform* is an integration in the $\mathbf{n}$-space over the closed surface Ω containing the origin, defined as :

$$f(\mathbf{x}) = R * (\hat{f}'') = -\frac{1}{8\pi^2} \int_{\Omega} \hat{f}''(\mathbf{n} \cdot \mathbf{x}, \mathbf{n}) d\Omega(\mathbf{n}) \qquad (A.2)$$

where :

$$\hat{f}''(\mathbf{n} \cdot \mathbf{x}, \mathbf{n}) = \left. \frac{\partial^2 \hat{f}(s,\mathbf{n})}{\partial s^2} \right|_{s=\mathbf{n}\cdot\mathbf{x}} \qquad (A.3)$$

Let $\delta(\mathbf{x}) = \delta(x_1, x_2, x_3)$ be the Dirac delta centered in the origin, i.e. the functional :

$$\int_{R^3} \delta(\mathbf{x}) f(\mathbf{x}) dV = f(\mathbf{o}) \qquad (A.4)$$

where $\mathbf{o}=(0,0,0)$.

We will use the same symbol δ for both one-dimensional and three-dimensional Dirac delta, with the convention that if the argument is a scalar, the one-dimensional Dirac delta is involved and if the argument is a vector, the three-dimensional Dirac delta is involved.

The Radon transform of the Dirac delta is :

$$\hat{\delta}(s,\mathbf{n}) = R[\delta(\mathbf{x})] = \int \delta(\mathbf{x}) \cdot \delta(s - \mathbf{n} \cdot \mathbf{x}) d\mathbf{x} = \delta(s - \mathbf{n} \cdot \mathbf{o}) = \delta(s) \qquad (A.5)$$

Now:

$$\frac{\partial \delta(\mathbf{n} \cdot \mathbf{x})}{\partial x_i} = \left. n_i \frac{d\delta}{ds} \right|_{s=\mathbf{n}\cdot\mathbf{x}} \quad ; \quad \frac{\partial^2 \delta(\mathbf{n} \cdot \mathbf{x})}{\partial x_i^2} = \left. n_i^2 \frac{d^2\delta}{d^2 s} \right|_{s=\mathbf{n}\cdot\mathbf{x}} \qquad (A.6.a,b)$$

Thus :

$$\sum_{i=1}^{3} \frac{\partial^2 \delta(\mathbf{n} \cdot \mathbf{x})}{\partial x_i^2} = \left. \sum_{i=1}^{3} n_i^2 \frac{d^2\delta}{ds^2} \right|_{s=\mathbf{n}\cdot\mathbf{x}} = \left. \frac{d^2\delta}{ds^2} \right|_{s=\mathbf{n}\cdot\mathbf{x}} \sum_{i=1}^{3} n_i^2 = \left. |\mathbf{n}|^2 \frac{d^2\delta}{ds^2} \right|_{s=\mathbf{n}\cdot\mathbf{x}} \qquad (A.7)$$

Since the first member of (A.7) is Laplacian of δ, $\Delta\delta$, Eq. (A.3) becomes:

$$\hat{\delta}'' = \left. \frac{d^2\delta}{ds^2} \right|_{s=\mathbf{n}\cdot\mathbf{x}} = \frac{\Delta\delta(\mathbf{n} \cdot \mathbf{x})}{|\mathbf{n}|^2} \qquad (A.8)$$

16

According to (A.2) the inverse Radon transform is :

$$\delta(\mathbf{x}) = -\frac{1}{8\pi^2} \int\limits_\Omega \frac{\Delta \delta(\mathbf{n}\cdot\mathbf{x})}{|\mathbf{n}|^2} d\Omega(\mathbf{n}) = -\frac{1}{8\pi^2} \Delta \int\limits_\Omega \frac{\delta(\mathbf{n}\cdot\mathbf{x})}{|\mathbf{n}|^2} d\Omega(\mathbf{n}) \qquad (A.9)$$

the last passage is due to the fact that the variable of integration is $\mathbf{n}$, not $\mathbf{x}$.

Thus, we have the very notable relation, called "plane representation for $\delta(\mathbf{x})$":

$$\delta(\mathbf{x}) = -\frac{1}{8\pi^2} \Delta \int\limits_\Omega \frac{\delta(\mathbf{n}\cdot\mathbf{x})}{|\mathbf{n}|^2} d\Omega(\mathbf{n}) \qquad (A.10)$$

that coincides with Eq. (6) in Wang [3].

11. Appendix B: Change of coordinate system

The Radon transform is an integration over the planes whose normal is $\mathbf{n}$. The inverse Radon transform, for a fixed $\mathbf{x}$, is an integration involving all the normal vectors $\mathbf{n}$. Therefore, a convenient coordinate system when we perform the inverse transform is such that an axis is parallel to $\mathbf{x}$ [3] (see Figure 1.a). Let us define:

$$r = |\mathbf{x}|; \quad \mathbf{e} = \frac{\mathbf{x}}{r} \qquad (B.1)$$

If $\mathbf{v}$ is an arbitrary unit vector different from $\mathbf{e}$ ($\mathbf{v} \neq \mathbf{e}$), two normal vectors orthogonal to $\mathbf{e}$ are :

$$\mathbf{p} = \frac{\mathbf{e}\times\mathbf{v}}{|\mathbf{e}\times\mathbf{v}|} \qquad (B.2)$$

$$\mathbf{q} = \mathbf{e}\times\mathbf{p} \qquad (B.3)$$

Let ξ, ζ, η be the components of *vector* $\mathbf{n}$ in the new coordinate system of R^3, then:

$$\mathbf{n} = \xi\mathbf{p} + \zeta\mathbf{q} + \eta\mathbf{e} \qquad (B.4a)$$

$$\mathbf{n}\cdot\mathbf{x} = \mathbf{p}\cdot\mathbf{x}\xi + \mathbf{q}\cdot\mathbf{x}\zeta + \mathbf{e}\cdot\mathbf{x}\eta = r\eta \qquad (B.4b)$$

This transformation induces a transformation of coordinates in the $\mathbf{n}$-space with (ξ, ζ, η) being the coordinates of *point* $\mathbf{n}$ in the new coordinate system in $\mathbf{n}$-space, see Figure 1.b. The determinant of the Jacobian of the latter transformation is obviously equal to 1.

12. Appendix C: coefficients b_{ijk}

If $\mathbf{v}=(1,0,0)$ then:

```
  b(1, 1, 1) = (yf**2*cd(5,5) - 2*yf*zf*cd(5,6) + zf**2*cd(6,6))/
  -(yf**2 + zf**2)
c
  b(1, 1, 2) = 2*(yf**3*cd(1,5) + yf*zf**2*cd(1,5)-yf**2*zf*cd(1,6)-
  -zf**3*cd(1,6) - xf*yf*zf*cd(5,5) - xf*yf**2*cd(5,6) +
  -xf*zf**2*cd(5,6) + xf*yf*zf*cd(6,6))/
  -((yf**2 + zf**2)*Sqrt(xf**2 + yf**2 + zf**2))
c
  b(1, 1, 3) = (yf**4*cd(1,1) +2*yf**2*zf**2*cd(1,1)+zf**4*cd(1,1)-
  -2*xf*yf**2*zf*cd(1,5)-2*xf*zf**3*cd(1,5)-2*xf*yf**3*cd(1,6)-
```

17

```
      -2*xf*yf*zf**2*cd(1,6) + xf**2*zf**2*cd(5,5)+2*xf**2*yf*zf*cd(5,6)+
      -xf**2*yf**2*cd(6,6))/((yf**2 + zf**2)*(xf**2 + yf**2 + zf**2))
c

      b(1, 2, 1) = (-(yf*zf*cd(2,5)) + zf**2*cd(2,6) + yf**2*cd(4,5) -
      -yf*zf*cd(4,6))/(yf**2 + zf**2)
c

      b(1, 2, 2) = (-(yf**2*zf*cd(1,2)) - zf**3*cd(1,2) + yf**3*cd(1,4)+
      -yf*zf**2*cd(1,4) - xf*yf**2*cd(2,5) + xf*zf**2*cd(2,5) +
      -2*xf*yf*zf*cd(2,6) - 2*xf*yf*zf*cd(4,5) - xf*yf**2*cd(4,6) +
      -xf*zf**2*cd(4,6) + yf**3*cd(5,6) + yf*zf**2*cd(5,6)-
      -yf**2*zf*cd(6,6) - zf**3*cd(6,6))/
      -((yf**2 + zf**2)*Sqrt(xf**2 + yf**2 + zf**2))
c

      b(1, 2, 3) = (-(xf*yf**3*cd(1,2)) - xf*yf*zf**2*cd(1,2) -
      -xf*yf**2*zf*cd(1,4) - xf*zf**3*cd(1,4) + yf**4*cd(1,6) +
      -2*yf**2*zf**2*cd(1,6) + zf**4*cd(1,6) + xf**2*yf*zf*cd(2,5) +
      -xf**2*yf**2*cd(2,6) + xf**2*zf**2*cd(4,5) + xf**2*yf*zf*cd(4,6) -
      -xf*yf**2*zf*cd(5,6) - xf*zf**3*cd(5,6) - xf*yf**3*cd(6,6) -
      -xf*yf*zf**2*cd(6,6))/((yf**2 + zf**2)*(xf**2 + yf**2 + zf**2))
c

      b(1, 3, 1) = (yf**2*cd(3,5) - yf*zf*cd(3,6) - yf*zf*cd(4,5) +
       -zf**2*cd(4,6))/(yf**2 + zf**2)
c

      b(1, 3, 2) = (yf**3*cd(1,3) + yf*zf**2*cd(1,3) - yf**2*zf*cd(1,4)-
      -zf**3*cd(1,4) - 2*xf*yf*zf*cd(3,5) - xf*yf**2*cd(3,6) +
      -xf*zf**2*cd(3,6) - xf*yf**2*cd(4,5) + xf*zf**2*cd(4,5) +
      -2*xf*yf*zf*cd(4,6) + yf**3*cd(5,5) + yf*zf**2*cd(5,5) -
      -yf**2*zf*cd(5,6) - zf**3*cd(5,6))/
      -((yf**2 + zf**2)*Sqrt(xf**2 + yf**2 + zf**2))
c

      b(1, 3, 3) = (-(xf*yf**2*zf*cd(1,3)) - xf*zf**3*cd(1,3)-
      -xf*yf**3*cd(1,4) -
      -xf*yf*zf**2*cd(1,4) + yf**4*cd(1,5) + 2*yf**2*zf**2*cd(1,5) +
      -zf**4*cd(1,5) + xf**2*zf**2*cd(3,5) + xf**2*yf*zf*cd(3,6) +
      -xf**2*yf*zf*cd(4,5) + xf**2*yf**2*cd(4,6) - xf*yf**2*zf*cd(5,5) -
      -xf*zf**3*cd(5,5) - xf*yf**3*cd(5,6) - xf*yf*zf**2*cd(5,6))/
      -((yf**2 + zf**2)*(xf**2 + yf**2 + zf**2))
c

      b(2, 1, 1) = b(1, 2, 1)
      b(2, 1, 2) = b(1, 2, 2)
      b(2, 1, 3) = b(1, 2, 3)
c

      b(2, 2, 1) = (zf**2*cd(2,2) - 2*yf*zf*cd(2,4) + yf**2*cd(4,4))/
       -(yf**2 + zf**2)
c

      b(2, 2, 2) = 2*(xf*yf*zf*cd(2,2) - xf*yf**2*cd(2,4) +
       -xf*zf**2*cd(2,4) -
      -yf**2*zf*cd(2,6) - zf**3*cd(2,6) -xf*yf*zf*cd(4,4) +yf**3*cd(4,6)+
      -yf*zf**2*cd(4,6))/((yf**2 + zf**2)*Sqrt(xf**2 + yf**2 + zf**2))
c

      b(2, 2, 3) = (xf**2*yf**2*cd(2,2) + 2*xf**2*yf*zf*cd(2,4) -
      -2*xf*yf**3*cd(2,6) - 2*xf*yf*zf**2*cd(2,6) + xf**2*zf**2*cd(4,4) -
      -2*xf*yf**2*zf*cd(4,6) - 2*xf*zf**3*cd(4,6) + yf**4*cd(6,6) +
      -2*yf**2*zf**2*cd(6,6) + zf**4*cd(6,6))/
      -((yf**2 + zf**2)*(xf**2 + yf**2 + zf**2))
c

      b(2, 3, 1) = (-(yf*zf*cd(2,3)) + zf**2*cd(2,4) + yf**2*cd(3,4) -
      -yf*zf*cd(4,4))/(yf**2 + zf**2)
c

      b(2, 3, 2) = (-(xf*yf**2*cd(2,3)) + xf*zf**2*cd(2,3) +
       -2*xf*yf*zf*cd(2,4) -
      -yf**2*zf*cd(2,5) - zf**3*cd(2,5)-2*xf*yf*zf*cd(3,4)+yf**3*cd(3,6)+
      -yf*zf**2*cd(3,6) - xf*yf**2*cd(4,4) + xf*zf**2*cd(4,4) +
      -yf**3*cd(4,5) + yf*zf**2*cd(4,5) -yf**2*zf*cd(4,6)-zf**3*cd(4,6))/
      -((yf**2 + zf**2)*Sqrt(xf**2 + yf**2 + zf**2))
c

      b(2, 3, 3) = (xf**2*yf*zf*cd(2,3) + xf**2*yf**2*cd(2,4) -
       -xf*yf**3*cd(2,5) -
      -xf*yf*zf**2*cd(2,5) + xf**2*zf**2*cd(3,4) - xf*yf**2*zf*cd(3,6) -
      -xf*zf**3*cd(3,6) + xf**2*yf*zf*cd(4,4) - xf*yf**2*zf*cd(4,5) -
      -xf*zf**3*cd(4,5) - xf*yf**3*cd(4,6) - xf*yf*zf**2*cd(4,6) +
      -yf**4*cd(5,6) + 2*yf**2*zf**2*cd(5,6) + zf**4*cd(5,6))/
      -((yf**2 + zf**2)*(xf**2 + yf**2 + zf**2))
c

      b(3, 1, 1) = b(1, 3, 1)
      b(3, 1, 2) = b(1, 3, 2)
      b(3, 1, 3) = b(1, 3, 3)
      b(3, 2, 1) = b(2, 3, 1)
      b(3, 2, 2) = b(2, 3, 2)
```

```
      b(3, 2, 3) = b(2, 3, 3)
c
      b(3, 3, 1) = (yf**2*cd(3,3) - 2*yf*zf*cd(3,4) + zf**2*cd(4,4))/
     -(yf**2 + zf**2)
c
      b(3, 3, 2) = 2*(-(xf*yf*zf*cd(3,3)) - xf*yf**2*cd(3,4) +
     -xf*zf**2*cd(3,4) +
     -yf**3*cd(3,5) + yf*zf**2*cd(3,5) + xf*yf*zf*cd(4,4) -
     -yf**2*zf*cd(4,5) - zf**3*cd(4,5))/
     -((yf**2 + zf**2)*Sqrt(xf**2 + yf**2 + zf**2))
c
      b(3, 3, 3) = (xf**2*zf**2*cd(3,3) + 2*xf**2*yf*zf*cd(3,4) -
     -2*xf*yf**2*zf*cd(3,5) - 2*xf*zf**3*cd(3,5) + xf**2*yf**2*cd(4,4) -
     -2*xf*yf**3*cd(4,5) - 2*xf*yf*zf**2*cd(4,5) + yf**4*cd(5,5) +
     -2*yf**2*zf**2*cd(5,5) + zf**4*cd(5,5))/
     -((yf**2 + zf**2)*(xf**2 + yf**2 + zf**2))
```

13. Appendix D: coefficients a_i

```
      a(1)=-(b(1,3,1)*b(2,2,1)*b(3,1,1))+
     -2*b(1,2,1)*b(2,3,1)*b(3,1,1)-
     -b(1,1,1)*b(2,3,1)*b(3,2,1)-
     -b(1,2,1)*b(2,1,1)*b(3,3,1)+
     -b(1,1,1)*b(2,2,1)*b(3,3,1);
c
      a(2)=-(b(1,3,2)*b(2,2,1)*b(3,1,1)+
     -b(1,3,1)*b(2,2,2)*b(3,1,1)+
     -b(1,3,1)*b(2,2,1)*b(3,1,2))+
     -2*(b(1,2,2)*b(2,3,1)*b(3,1,1)+
     -b(1,2,1)*b(2,3,2)*b(3,1,1)+
     -b(1,2,1)*b(2,3,1)*b(3,1,2))-
     -(b(1,1,2)*b(2,3,1)*b(3,2,1)+
     -b(1,1,1)*b(2,3,2)*b(3,2,1)+
     -b(1,1,1)*b(2,3,1)*b(3,2,2))-
     -(b(1,2,2)*b(2,1,1)*b(3,3,1)+
     -b(1,2,1)*b(2,1,2)*b(3,3,1)+
     -b(1,2,1)*b(2,1,1)*b(3,3,2))+
     -(b(1,1,2)*b(2,2,1)*b(3,3,1)+
     -b(1,1,1)*b(2,2,2)*b(3,3,1)+
     -b(1,1,1)*b(2,2,1)*b(3,3,2));
c
      a(3)=-(b(1,3,3)*b(2,2,1)*b(3,1,1)+
     -b(1,3,1)*b(2,2,3)*b(3,1,1)+
     -b(1,3,1)*b(2,2,1)*b(3,1,3)+
     -b(1,3,2)*b(2,2,2)*b(3,1,1)+
     -b(1,3,1)*b(2,2,2)*b(3,1,2)+
     -b(1,3,2)*b(2,2,1)*b(3,1,2))+
     -2*(b(1,2,3)*b(2,3,1)*b(3,1,1)+
     -b(1,2,1)*b(2,3,3)*b(3,1,1)+
     -b(1,2,1)*b(2,3,1)*b(3,1,3)+
     -b(1,2,2)*b(2,3,2)*b(3,1,1)+
     -b(1,2,1)*b(2,3,2)*b(3,1,2)+
     -b(1,2,2)*b(2,3,1)*b(3,1,2))-
     -(b(1,1,3)*b(2,3,1)*b(3,2,1)+
     -b(1,1,1)*b(2,3,3)*b(3,2,1)+
     -b(1,1,1)*b(2,3,1)*b(3,2,3)+
     -b(1,1,2)*b(2,3,2)*b(3,2,1)+
     -b(1,1,1)*b(2,3,2)*b(3,2,2)+
     -b(1,1,2)*b(2,3,1)*b(3,2,2))-
     -(b(1,2,3)*b(2,1,1)*b(3,3,1)+
     -b(1,2,1)*b(2,1,3)*b(3,3,1)+
     -b(1,2,1)*b(2,1,1)*b(3,3,3)+
     -b(1,2,2)*b(2,1,2)*b(3,3,1)+
     -b(1,2,1)*b(2,1,2)*b(3,3,2)+
     -b(1,2,2)*b(2,1,1)*b(3,3,2))+
     -(b(1,1,3)*b(2,2,1)*b(3,3,1)+
     -b(1,1,1)*b(2,2,3)*b(3,3,1)+
     -b(1,1,1)*b(2,2,1)*b(3,3,3)+
     -b(1,1,2)*b(2,2,2)*b(3,3,1)+
     -b(1,1,1)*b(2,2,2)*b(3,3,2)+
     -b(1,1,2)*b(2,2,1)*b(3,3,2))
c
      a(4)=-(b(1,3,3)*b(2,2,2)*b(3,1,1)+
     -b(1,3,2)*b(2,2,3)*b(3,1,1)+
     -b(1,3,1)*b(2,2,2)*b(3,1,3)+
     -b(1,3,1)*b(2,2,3)*b(3,1,2)+
     -b(1,3,2)*b(2,2,1)*b(3,1,3)+
```

```
        -b(1,3,3)*b(2,2,1)*b(3,1,2)+
        -b(1,3,2)*b(2,2,2)*b(3,1,2))+
        -2*(b(1,2,3)*b(2,3,2)*b(3,1,1)+
        -b(1,2,2)*b(2,3,3)*b(3,1,1)+
        -b(1,2,1)*b(2,3,2)*b(3,1,3)+
        -b(1,2,1)*b(2,3,3)*b(3,1,2)+
        -b(1,2,2)*b(2,3,1)*b(3,1,3)+
        -b(1,2,3)*b(2,3,1)*b(3,1,2)+
        -b(1,2,2)*b(2,3,2)*b(3,1,2))-
        -(b(1,1,3)*b(2,3,2)*b(3,2,1)+
        -b(1,1,2)*b(2,3,3)*b(3,2,1)+
        -b(1,1,1)*b(2,3,2)*b(3,2,3)+
        -b(1,1,1)*b(2,3,3)*b(3,2,2)+
        -b(1,1,2)*b(2,3,1)*b(3,2,3)+
        -b(1,1,3)*b(2,3,1)*b(3,2,2)+
        -b(1,1,2)*b(2,3,2)*b(3,2,2))-
        -(b(1,2,3)*b(2,1,2)*b(3,3,1)+
        -b(1,2,2)*b(2,1,3)*b(3,3,1)+
        -b(1,2,1)*b(2,1,2)*b(3,3,3)+
        -b(1,2,1)*b(2,1,3)*b(3,3,2)+
        -b(1,2,2)*b(2,1,1)*b(3,3,3)+
        -b(1,2,3)*b(2,1,1)*b(3,3,2)+
        -b(1,2,2)*b(2,1,2)*b(3,3,2))+
        -(b(1,1,3)*b(2,2,2)*b(3,3,1)+
        -b(1,1,2)*b(2,2,3)*b(3,3,1)+
        -b(1,1,1)*b(2,2,2)*b(3,3,3)+
        -b(1,1,1)*b(2,2,3)*b(3,3,2)+
        -b(1,1,2)*b(2,2,1)*b(3,3,3)+
        -b(1,1,3)*b(2,2,1)*b(3,3,2)+
        -b(1,1,2)*b(2,2,2)*b(3,3,2))
c
        a(5)=-(b(1,3,2)*b(2,2,2)*b(3,1,3)+
        -b(1,3,3)*b(2,2,2)*b(3,1,2)+
        -b(1,3,2)*b(2,2,3)*b(3,1,2)+
        -b(1,3,1)*b(2,2,3)*b(3,1,3)+
        -b(1,3,3)*b(2,2,1)*b(3,1,3)+
        -b(1,3,3)*b(2,2,3)*b(3,1,1))+
        -2*(b(1,2,2)*b(2,3,2)*b(3,1,3)+
        -b(1,2,3)*b(2,3,2)*b(3,1,2)+
        -b(1,2,2)*b(2,3,3)*b(3,1,2)+
        -b(1,2,1)*b(2,3,3)*b(3,1,3)+
        -b(1,2,3)*b(2,3,1)*b(3,1,3)+
        -b(1,2,3)*b(2,3,3)*b(3,1,1))-
        -(b(1,1,2)*b(2,3,2)*b(3,2,3)+
        -b(1,1,3)*b(2,3,2)*b(3,2,2)+
        -b(1,1,2)*b(2,3,3)*b(3,2,2)+
        -b(1,1,1)*b(2,3,3)*b(3,2,3)+
        -b(1,1,3)*b(2,3,1)*b(3,2,3)+
        -b(1,1,3)*b(2,3,3)*b(3,2,1))-
        -(b(1,2,2)*b(2,1,2)*b(3,3,3)+
        -b(1,2,3)*b(2,1,2)*b(3,3,2)+
        -b(1,2,2)*b(2,1,3)*b(3,3,2)+
        -b(1,2,1)*b(2,1,3)*b(3,3,3)+
        -b(1,2,3)*b(2,1,1)*b(3,3,3)+
        -b(1,2,3)*b(2,1,3)*b(3,3,1))+
        -(b(1,1,2)*b(2,2,2)*b(3,3,3)+
        -b(1,1,3)*b(2,2,2)*b(3,3,2)+
        -b(1,1,2)*b(2,2,3)*b(3,3,2)+
        -b(1,1,1)*b(2,2,3)*b(3,3,3)+
        -b(1,1,3)*b(2,2,1)*b(3,3,3)+
        -b(1,1,3)*b(2,2,3)*b(3,3,1))
c
        a(6)=-(b(1,3,2)*b(2,2,3)*b(3,1,3)+
        -b(1,3,3)*b(2,2,2)*b(3,1,3)+
        -b(1,3,3)*b(2,2,3)*b(3,1,2))+
        -2*(b(1,2,2)*b(2,3,3)*b(3,1,3)+
        -b(1,2,3)*b(2,3,2)*b(3,1,3)+
        -b(1,2,3)*b(2,3,3)*b(3,1,2))-
        -(b(1,1,2)*b(2,3,3)*b(3,2,3)+
        -b(1,1,3)*b(2,3,2)*b(3,2,3)+
        -b(1,1,3)*b(2,3,3)*b(3,2,2))-
        -(b(1,2,2)*b(2,1,3)*b(3,3,3)+
        -b(1,2,3)*b(2,1,2)*b(3,3,3)+
        -b(1,2,3)*b(2,1,3)*b(3,3,2)+
        -(b(1,1,2)*b(2,2,3)*b(3,3,3)+
        -b(1,1,3)*b(2,2,2)*b(3,3,3)+
        -b(1,1,3)*b(2,2,3)*b(3,3,2))
c
        a(7)=-(b(1,3,3)*b(2,2,3)*b(3,1,3))+
```

```
-2*b(1,2,3)*b(2,3,3)*b(3,1,3)-
-b(1,1,3)*b(2,3,3)*b(3,2,3)-
-b(1,2,3)*b(2,1,3)*b(3,3,3)+
-b(1,1,3)*b(2,2,3)*b(3,3,3)
```

Figure captions:

Fig. 1.a. Anisotropic elastic body (shown bounded for representation convenience) referred to a fixed Cartesian system.

Fig. 1.b. Closed surface Ω containing the origin in the **n**-space.

Fig. 2. Parallelepiped over which contour integration is taken in the **n**-space; Surfaces S_1 and S_2 are bounded by $\xi=\pm 1$, S_3 and S_4 by $\zeta=\pm L$, S_5 and S_6 by $\eta=\pm L$.

Fig. 3. Cube having edge of length $l=1$ m discretized with six nine-node quadrilateral elements with a total of 26 nodes.

Fig. 4. Orientation of the plane of transverse isotropy. Dip angle ψ is the angle between the plane of symmetry and x_1x_2 plane; dip direction angle φ is the angle between x_2 and the orthogonal projection of the dip vector on the x_1x_2 plane. Positive angles are shown.
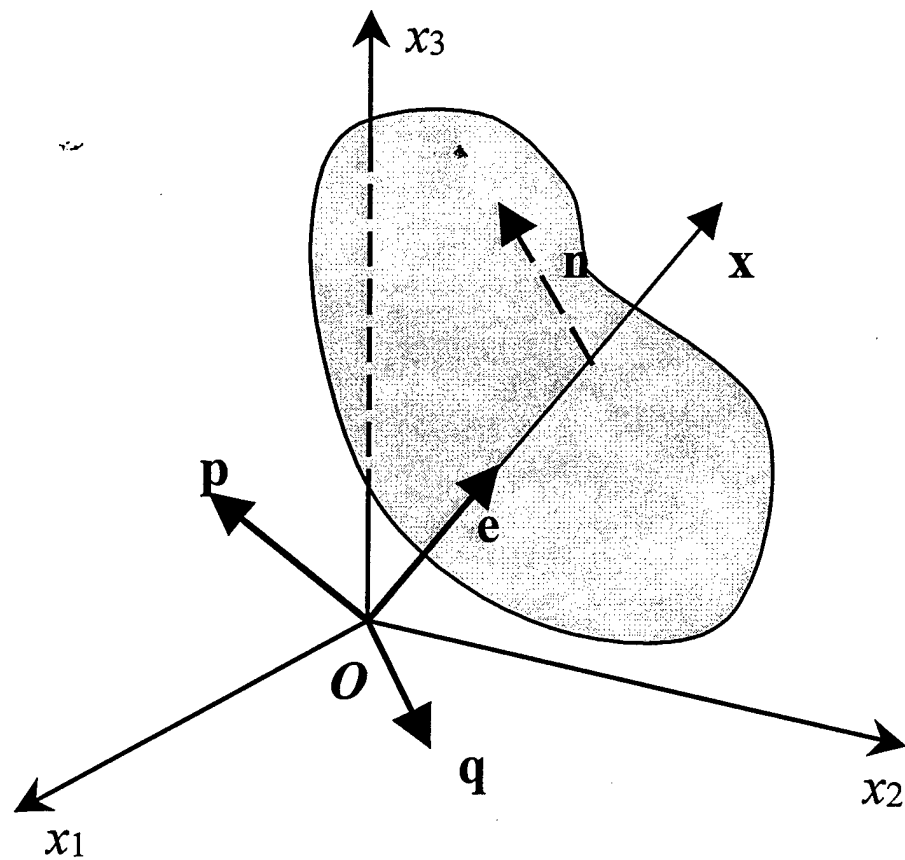
Fig. 1.a. Anisotropic elastic body (shown bounded for representation convenience) referred to a fixed Cartesian system. Vectors **p**, **q**, and **e** are defined in Appendix B.
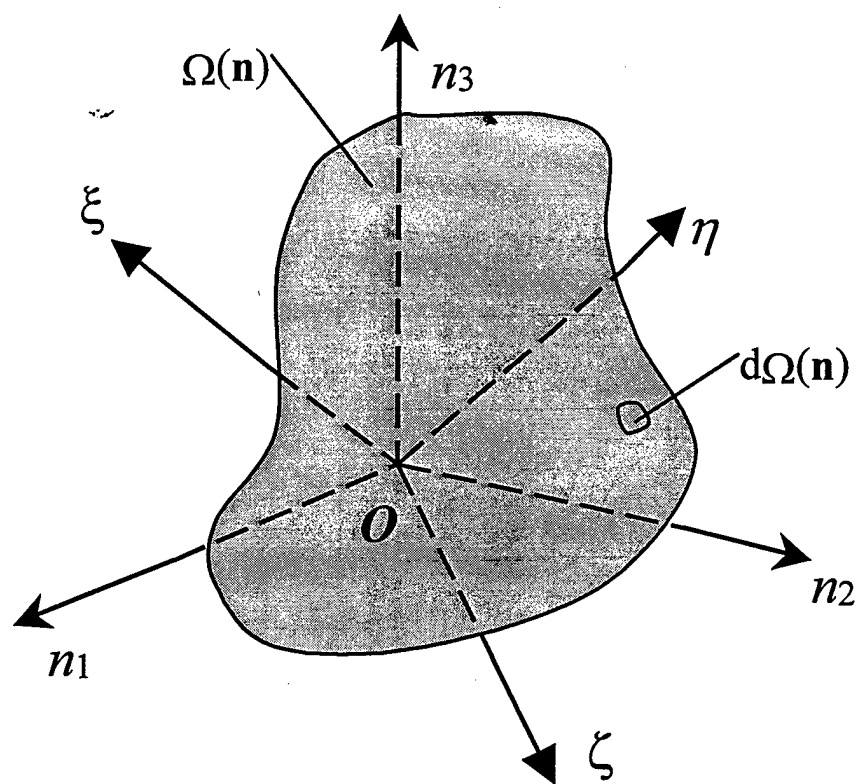
Fig. 1.b. Closed surface Ω containing the origin in the **n**-space.
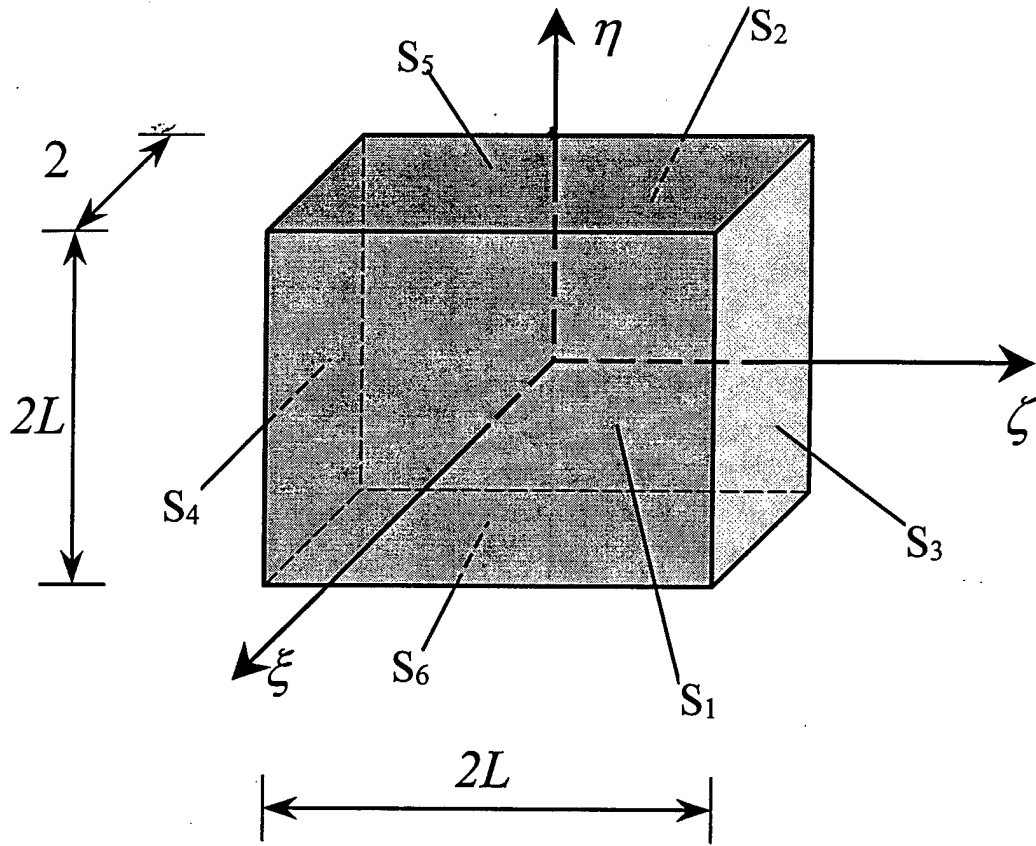
Fig. 2. Parallelepiped over which contour integration is taken in the **n**-space; Surfaces S_1 and S_2 are bounded by $\xi=\pm 1$, S_3 and S_4 by $\zeta=\pm L$, S_5 and S_6 by $\eta=\pm L$.
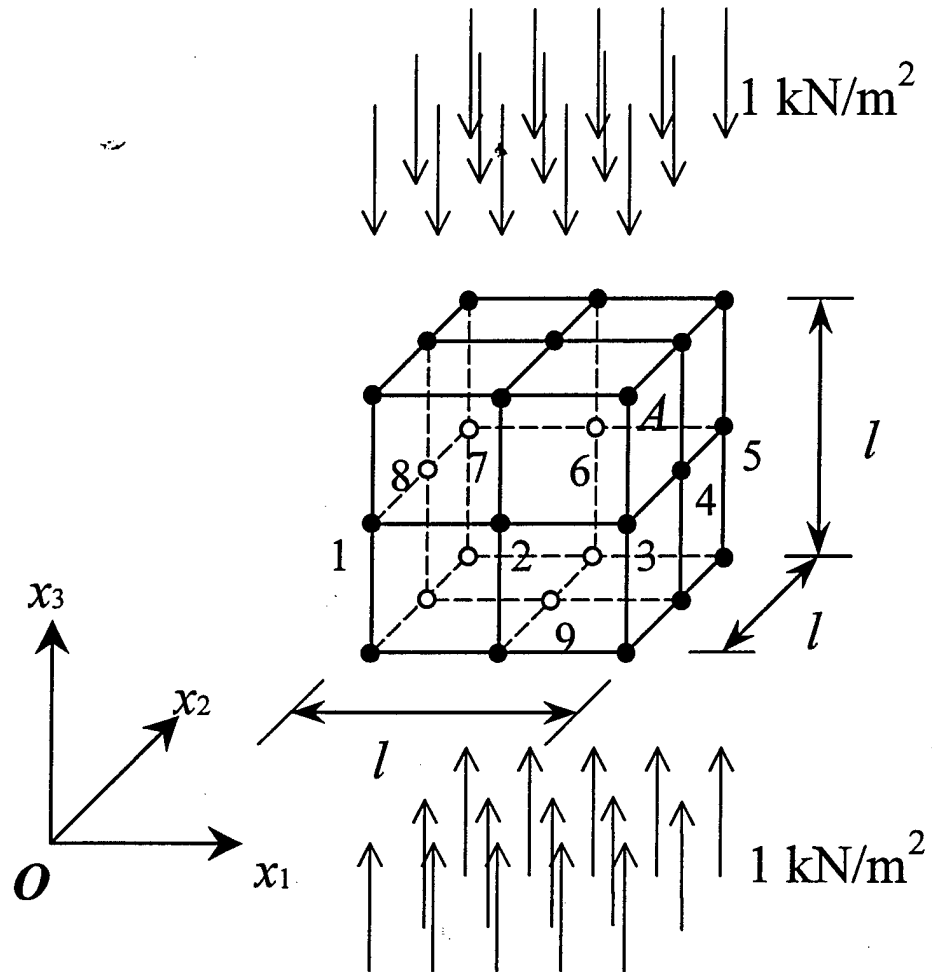
Fig. 3. Cube having edge of length l=1 m discretized with six nine-node quadrilateral elements with a total of 26 nodes. Nodes from 1 to 8 have fixed displacement along x_3, node 9 has fixed displacements along x_1 and x_2.
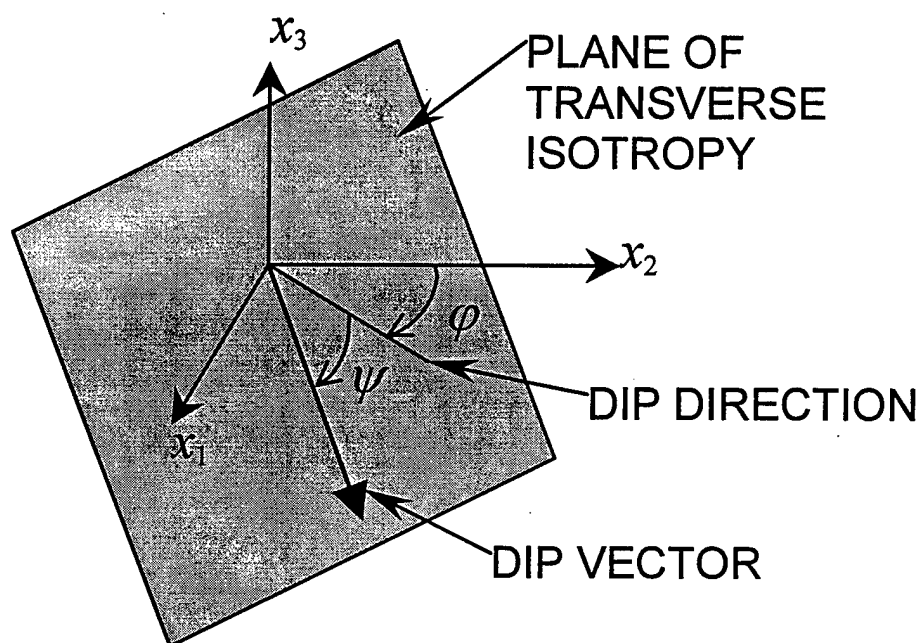
Fig. 4. Orientation of the plane of transverse isotropy. Dip angle ψ is the angle between the plane of symmetry and x_1x_2 plane; dip direction angle φ is the angle between x_2 and the orthogonal projection of the dip vector on the x_1x_2 plane. Positive angles are shown.

Table captions

Table 1. Correspondence between notation used in the text and notation used in the Fortran code.

Table 2. Green's displacements (m^{-4}) calculated according to the closed-form solution of Pan and Chou [4] and the present formulation.

Table 3. Green's stresses (kN/m^2) calculated according to the closed-form solution of Pan and Chou [4] and the present formulation.

Table 4. Derivatives of the Green's stresses (kN/m^2) calculated according to the closed-form solution of Pan and Chou [4] and the present formulation.

Table 5. Block under uniform compression. Example 1: surface displacements at node A ($x10^{-5}$ m).

Table 6.1. Block under uniform compression. Example 1: internal displacements along the vertical center line.

Table 6.2. Block under uniform compression. Example 1: stresses along the vertical center line.

Table 6.3. Block under uniform compression. Example 1: stresses along the vertical center line.

Table 6.4. Block under uniform compression. Example 1: stresses along the vertical center line.

Table 7. Zinc block under uniform compression. Example 2: boundary displacements at node A ($x10^{-7}$ m).

Table 1. Correspondence between notation used in the text and notation used in the present FORTRAN code.

Notation used in the text	Notation used in the Fortran code
b_{ijk}	b(i,j,k)
D_{ij}	cd(i,j)
$\mathbf{x}=(x_1, x_2, x_3)$	xf, yf, zf
a_i	a(i)

Table 2. Green's displacements (m^{-4}) calculated according to Pan's and Chou's closed-form solution [4] as implemented in [11] and with the present formulation. The source point is at the origin, the field point is at $\mathbf{x}=(-1,0.8,1.5)$ m.

(I,j)	g_{ij} transversely isotropic formulation	g_{ij} present formulation	relative difference
1,1	4.0141588565E-03	4.0141588610E-03	1.1E-09
1,2	-2.9315529284E-04	-2.9315529143E-04	4.8E-09
1,3	-2.1517885087E-03	-2.1517885172E-03	3.9E-09
2,1	-2.9315529284E-04	-2.9315529143E-04	4.8E-09
2,2	3.8822389747E-03	3.8822389799E-03	1.3E-09
2,3	1.7214308070E-03	1.7214308137E-03	3.9E-09
3,1	-2.1517885087E-03	-2.1517885172E-03	3.9E-09
3,2	1.7214308070E-03	1.7214308137E-03	3.9E-09
3,3	1.9003220124E-02	1.9003220284E-02	8.4E-09

Table 3. Green's stresses (kN/m^2) calculated according to Pan's and Chou's closed-form solution [4] as implemented in [11] and the present formulation. The source point is at the origin, the field point in x=(-1,0.8,1.5) m.

ijk	σ_{ijk} transversely isotropic formulation	σ_{ijk} present formulation	relative difference
111	3.0534645334E-03	3.0534575287E-03	2.3E-06
221	5.5516532436E-03	5.5516460542E-03	1.3E-06
331	6.9594542712E-03	6.9594505349E-03	5.4E-07
231	2.5160305656E-03	2.5160307422E-03	7.0E-08
131	-3.3933330101E-03	-3.3933332396E-03	6.8E-08
121	-1.8033628216E-03	-1.8033626725E-03	8.3E-08
111	-5.6717491681E-03	-5.6717487868E-03	6.7E-08
221	-1.2123450534E-03	-1.2123450967E-03	3.6E-08
331	-5.5675634169E-03	-5.5675634915E-03	1.3E-08
231	-2.2611192556E-03	-2.2611192104E-03	2.0E-08
131	2.5160305656E-03	2.5160306251E-03	2.4E-08
121	7.1617031049E-04	7.1617003567E-04	3.8E-07
111	-1.7147827999E-02	-1.7147807646E-02	1.2E-06
221	-8.3655438558E-03	-8.3655210747E-03	2.7E-06
331	-2.2078536037E-02	-2.2078524002E-02	5.4E-07
231	-1.1775219220E-02	-1.1775219467E-02	2.1E-08
131	1.4719024025E-02	1.4719024871E-02	5.7E-08
121	1.9516186984E-02	1.9516189072E-02	1.1E-07

Table 4. Derivatives of the Green's stresses (kN/m^3) calculated according to Pan's and Chou's closed-form solution [4] as implemented in [11] and the present formulation. The source point is at the origin, the field point in **x**=(-1,0.8,1.5) m.

Ijk,l	$\sigma_{ijk,l}$ transversely isotropic formulation	$\sigma_{ijk,l}$ present formulation	relative difference
111,1	-0.59622259271E-02	-0.59629572705E-02	1.2E-04
111,2	-0.45086940696E-02	-0.45074656599E-02	-2.7E-04
111,3	-0.56414664921E-02	-0.56411267186E-02	-6.0E-05
221,1	0.44694421882E-02	0.44685063303E-02	-2.0E-04
221,2	-0.11811731607E-02	-0.11798500052E-02	-1.1E-03
221,3	-0.37926171802E-02	-0.37921063932E-02	-1.3E-04
331,1	0.16987884233E-02	0.16982433466E-02	-3.2E-04
331,2	-0.69265941556E-02	-0.69258768984E-02	-1.0E-04
331,3	-0.44525631963E-02	-0.44523121121E-02	-5.6E-05
231,1	0.79385810234E-03	0.79379727638E-03	-7.7E-05
231,2	0.49712727263E-03	0.49714271358E-03	3.1E-05
231,3	-0.30906032310E-02	-0.30906216080E-02	5.9E-06
131,1	0.39554359236E-02	0.39554842055E-02	1.2E-05
131,2	0.18677123922E-02	0.18676962357E-02	-8.6E-06
131,3	0.61652880201E-02	0.61653303015E-02	6.8E-06
121,1	0.42717763920E-02	0.42718112393E-02	8.1E-06
121,2	-0.20306209291E-03	-0.20300240322E-03	-2.9E-04
121,3	0.53606344730E-02	0.53607252836E-02	1.7E-05
112,1	-0.30768883497E-02	-0.30775369921E-02	2.1E-04
112,2	0.84038676742E-03	0.84094663232E-03	6.7E-04
112,3	0.50628670483E-02	0.50629208004E-02	1.6E-05
222,1	-0.26129788805E-02	-0.26137365442E-02	2.9E-04
222,2	-0.48936107600E-02	-0.48931499059E-02	-9.4E-05
222,3	0.24843998895E-02	0.24845314971E-02	5.3E-05
332,1	-0.69265941556E-02	-0.69269468094E-02	5.9E-05
332,2	-0.14181789466E-02	-0.14179740950E-02	-1.4E-04
332,3	0.35620505570E-02	0.35621376993E-02	2.4E-05
232,1	-0.84519058971E-03	-0.84518000388E-03	-1.2E-05
232,2	-0.43559086593E-02	-0.43559177742E-02	2.9E-06
232,3	0.47745165660E-02	0.47746037165E-02	1.8E-05
132,1	0.79385810234E-03	0.79378559587E-03	-9.1E-05
132,2	0.49712727263E-03	0.49718754586E-03	1.2E-04
132,3	-0.30906032312E-02	-0.30906169537E-02	4.4E-06
122,1	0.11909419404E-03	0.11905631360E-03	-3.2E-04
122,2	0.61674915810E-02	0.61674862040E-02	-8.7E-07
122,3	-0.41648264611E-02	-0.41648490465E-02	5.4E-06
113,1	0.71134008460E-02	0.71131995957E-02	-2.8E-05
113,2	0.33341653291E-01	0.33342792915E-01	3.4E-05
113,3	0.98238228068E-02	0.98259170804E-02	2.1E-04
223,1	-0.29318534460E-01	-0.29319149219E-01	3.0E-05
223,2	-0.15577546399E-01	-0.15576273564E-01	-8.2E-05
223,3	-0.83606419668E-04	-0.81186914690E-04	-2.9E-02
333,1	-0.27302017639E-01	-0.27302079852E-01	2.3E-06
333,2	0.21841614111E-01	0.21842236628E-01	2.8E-05
333,3	-0.41215790310E-03	-0.41093285237E-03	-3.0E-03
233,1	-0.14561076074E-01	-0.14560962479E-01	-7.8E-06
233,2	-0.30701631651E-02	-0.30703156075E-02	5.0E-05
233,3	0.76303285982E-02	0.76304202029E-02	1.2E-05
133,1	0.34823210683E-02	0.34819436621E-02	-1.1E-04
133,2	-0.14561076074E-01	-0.14560935326E-01	-9.7E-06
131,3	-0.95379107477E-02	-0.95379106793E-02	-7.2E-09
123,1	0.79472178014E-02	0.79465584372E-02	-8.3E-05
123,2	0.24245099017E-02	0.24250012946E-02	2.3E-04
123,3	-0.22016509392E-01	-0.22016463462E-01	-2.1E-06

Table 5. Block under uniform compression. Example 1: surface displacements at node A $(\times 10^{-5}$ m).

	Present	Transv. isotropic form. [11]	Exact [12]
u_1	-0.5496	-0.5496	-0.5496
u_2	-0.7029	-0.7032	-0.7031
u_3	-1.0417	-1.0417	-1.0417

Table 6.1. Block under uniform compression. Example 1: internal displacements along the vertical center line.

z(m)	u_3 $(\times 10^{-5}$ m)		
	Present	Transv. isotropic form. [11]	Exact [12]
0.75	-0.5210	-0.5208	-0.5209
0.625	-0.2604	-0.2604	-0.2604
0.5	0.0000	0.0000	0.0000
0.375	0.2604	0.2604	0.2604
0.25	0.5208	0.5208	0.5208

Table 6.2. Block under uniform compression. Example 1: stresses along the vertical center line.

z(m)	σ_{11} (kN/m^2)		
	Present	Transv. isotropic form. [11]	Exact [12]
0.75	0.0005	0.0011	0.0000
0.625	0.0006	-0.0000	0.0000
0.5	-0.0023	-0.0000	0.0000
0.375	0.0096	-0.0000	0.0000
0.25	0.0013	0.0014	0.0000

32

Table 6.3. Block under uniform compression. Example 1: stresses along the vertical center line.

z(m)	σ_{22} (kN/m^2)		
	Present	Transv. isotropic form. [11]	Exact [12]
0.75	-0.0060	-0.0040	0.0000
0.625	-0.0021	-0.0000	0.0000
0.5	-0.0007	0.0000	0.0000
0.375	0.0084	-0.0000	0.0000
0.25	-0.0045	-0.0044	0.0000

Table 6.4. Block under uniform compression. Example 1: stresses along the vertical center line.

z(m)	σ_{33} (kN/m^2)		
	Present	Transv. isotropic form. [11]	Exact [12]
0.75	-0.999	-1.001	-1.000
0.625	-0.992	-1.000	-1.000
0.5	-1.002	-1.000	-1.000
0.375	-1.000	-1.000	-1.000
0.25	-1.003	0.988	-1.000

Table 7. Zinc block under uniform compression. Example 2: boundary displacements at node A (x10^{-7} m).

	Present	Anisotropic formulation [13]	Exact [12]
u_1	7.278	7.291	7.274
u_2	-7.277	-7.291	-7.274
u_3	-28.35	-28.42	-28.34